AD-A060 735 NAVAL RESEARCH LAB WASHINGTON D C F/G 20/8
TEMPORAL DEUTERON CURRENT DETERMINATIONS USING NEUTRON TIME-OF---ETC(U)
AUG 78 F C YOUNG, S J STEPHANAKIS

UNCLASSIFIED NRL-MR-3823 SBIE-AD-E000 229 NL

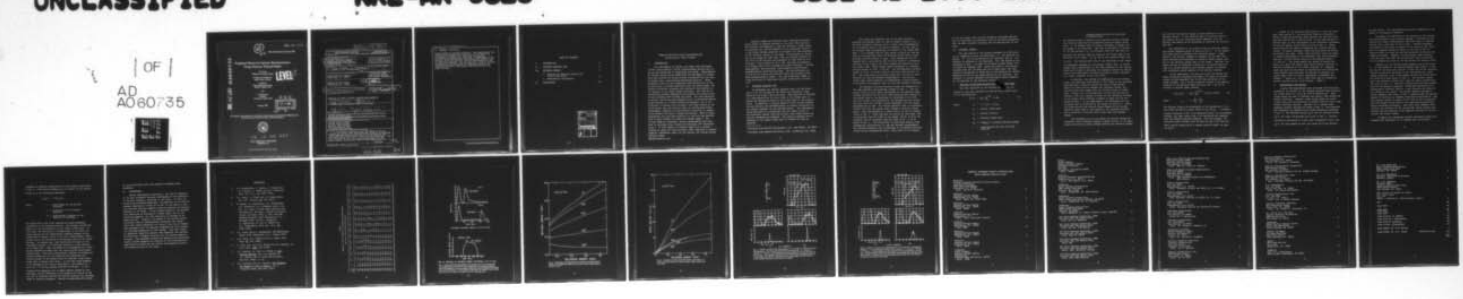

END
DATE FILMED
01-79
DDC

NRL Memorandum Report 3823

Temporal Deuteron Current Determinations Using Neutron Time-of-Flight

F.C. Young
Radiation Technology Division

D. Mosher, S.J. Stephanakis
Plasma Physics Division

S. Goldstein
Science Applications Branch
McLean, Virginia 22101

and

D. Hinshelwood
JAYCOR
Alexandria, Virginia 22304

August 1978

This Research was Sponsored by the Defense Nuclear Agency Under Subtask T99QAXLA014, Work Unit 46, and Work Unit Title Ion Beam Generation.

NAVAL RESEARCH LABORATORY
Washington, D.C.

(14) NRL-MR-3823

SECURITY CLASSIFICATION OF THIS PAGE (When Data Entered)

REPORT DOCUMENTATION PAGE

READ INSTRUCTIONS BEFORE COMPLETING FORM

1. REPORT NUMBER: NRL Memorandum Report 3823
2. GOVT ACCESSION NO.
3. RECIPIENT'S CATALOG NUMBER

(6) 4. TITLE (and Subtitle): TEMPORAL DEUTERON CURRENT DETERMINATIONS USING NEUTRON TIME-OF-FLIGHT

5. TYPE OF REPORT & PERIOD COVERED: Interim report on a continuing NRL Problem
6. PERFORMING ORG. REPORT NUMBER

7. AUTHOR(s): F.C. Young, D. Mosher, S.J. Stephanakis, S. Goldstein and D. Hinshelwood
8. CONTRACT OR GRANT NUMBER(s): (9) Memorandum rept.

9. PERFORMING ORGANIZATION NAME AND ADDRESS: Naval Research Laboratory, Washington, D.C. 20375
10. PROGRAM ELEMENT, PROJECT, TASK AREA & WORK UNIT NUMBERS: NRL Problem H02-26A, DNA Subtask T99QAXLA014

11. CONTROLLING OFFICE NAME AND ADDRESS: Defense Nuclear Agency, Washington, D.C. 20305
(11) 12. REPORT DATE: Aug 1978
13. NUMBER OF PAGES: 25

14. MONITORING AGENCY NAME & ADDRESS (if different from Controlling Office)
15. SECURITY CLASS. (of this report): UNCLASSIFIED
15a. DECLASSIFICATION/DOWNGRADING SCHEDULE

(12) 26p.

(10) Frank C./Young, Stavros J./Stephanakis, S./Goldstein D./Hinshelwood

16. DISTRIBUTION STATEMENT (of this Report)

Approved for public release; distribution unlimited.

(16) T99QAXL (17) AØ14

17. DISTRIBUTION STATEMENT (of the abstract entered in Block 20, if different from Report)

(18) SRIE (19) AD-EØØØ229

18. SUPPLEMENTARY NOTES

This research was sponsored by the Defense Nuclear Agency under subtask T99QAXLA014, work unit 46, and work unit title Ion Beam Generation.
This report contains the text of a paper presented at the 1978 IEEE International Conference on Plasma Science, Monterey, California, May 1978.

19. KEY WORDS (Continue on reverse side if necessary and identify by block number)

Intense Deuteron Beams
Neutron Time-of-Flight
Deuteron Pulse Duration
Deuteron Emission Time
d(d,n)^{3}He Cross Sections

20. ABSTRACT (Continue on reverse side if necessary and identify by block number)

In experiments conducted on the NRL Gamble II device, focused-ion currents have previously been inferred by combining time-integrated neutron yield data with time-resolved diode electrical characteristics in a model for ion production. The time variation of ion current can be determined in a more direct fashion from neutron time-of-flight measurements at

continues

251 950

20. ABSTRACT (continued)

various angles to the beam direction. Such measurements have recently been successfully carried out in the hard x-ray environment of Gamble II by employing fast-recovery scintillator-photomultiplier detectors. Measurements of the deuteron energy and emission time deduced from neutron time-of-flight are consistent with current understanding of the ion generation process. The ion current vs. time is unfolded from measured neutron signals by combining them with the temporally-resolved diode voltage and neutron-production cross sections.

TABLE OF CONTENTS

I.	INTRODUCTION	1
II.	DEUTERON EMISSION TIME	2
III.	DEUTERON CURRENT	4
	1. Relation of Deuteron Current and Neutron TOF Yield	4
	2. Measurements and Results	7
IV.	CONCLUSIONS	10

Temporal Deuteron Current Determinations Using Neutron Time-of-Flight

I. INTRODUCTION

The development of intense ion beams from high-power (10^{12}W) short-duration (10^{-8}s) pulsed-plasma sources has required new approaches to diagnosing such beams. Measurements[1] of intense pulsed proton beams from the NRL Gamble II pulser have been carried out using nuclear activation[2] and ion time-of-flight with a scintillator-photodiode detector. These techniques have not been completely satisfactory due to the intense burst of energy associated with the proton beam. The nuclear activation technique was limited by the ablation of the surface of the target being activated. Only the use of attenuating screens eliminated this problem for proton intensities exceeding 10^{16} protons per pulse. The time variation of proton current has been measured with a scintillator-photodiode detector in a time-of-flight arrangement, but it is difficult to provide a sufficiently thin light shield on the scintillator that can survive these ion intensities intact. Furthermore, magnetic or electrostatic deflection is complicated because the beam is charge neutralized. Both of these diagnostics are even more difficult to use with the development of more intense ion beams and focused beams.[3] For focused beams of deuterons, neutron measurements have been used to determine beam intensities exceeding 10^{17} deuterons/pulse.[3] In this report, we present results of a neutron diagnostic using the time-of-flight (TOF) technique to provide temporal information about the ion current for intense pulsed deuteron beams.

Manuscript submitted July 3, 1978.

Deuteron beams are directed onto a deuterated polyethylene target to produce neutrons by the $d(d,n)^3He$ reaction. The neutrons are measured in time for different flight paths to determine the time-of-emission of the deuterons relative to the diode voltage pulse and to evaluate the time variation of the deuteron current in the beam. The energies of deuterons in the beams are less than 1 MeV so neutrons produced by the $^{12}C(d,n)^{13}N$ reaction are separated in time from the d-d neutrons. Total yields of up to 10^{11} neutrons are measured on a single shot with a rhodium activation detector.[4] For TOF measurements, fast-recovery, high-linearity scintillator-photomultiplier detectors are used. The scintillators are 6.7-cm dia by 5.6-cm thick NE-111* which are mounted on XP-2020 photomultiplier tubes†. The time resolution (FWHM) of these detectors to individual neutron interactions is about 5 ns.

II. DEUTERON EMISSION TIME

To determine the neutron emission time, two TOF detectors at 15° to the axis of the diode with different flight paths of 1.91 m and 7.42 m are used. Each detector is enclosed in a lead shield with 2.5 cm of lead in the flight path to reduce the saturation level of the x-ray flash in the scintillator. In addition, a neutral density filter is used between the scintillator and photomultiplier to prevent saturation of the neutron response in the photomultiplier. The responses of these detectors on a particular shot are shown in Fig. 1. The detectors recover from the initial x-ray flash before the neutron responses are measured. The neutron response corresponding to the longer flight path is delayed in time as expected.

---

*Available from Nuclear Enterprises, Ltd., San Carlos, CA, 94070

†Available from Amperex Electronic Corp., Hicksville, NY, 11802

The energy and emission time of the most energetic neutrons are deduced from the time-of-flight traces in Fig. 1. The most energetic neutrons have a flight time corresponding to the leading edge of the neutron response. We use time on the leading edge corresponding to one-half of the signal maximum. It is assumed that no high energy neutrons are emitted late in the pulse and reach the detector before lower energy neutrons emitted earlier in time. This assumption will be checked later. The neutron time for each detector is measured relative to the peak of the x-ray signal and corrected for x-ray flight time. These flight times correspond to a maximum neutron energy of 3.41 ± 0.15 MeV. The corresponding deuteron energy is 0.45 ± 0.10 MeV based on the $d(d,n)^3He$ reaction at 15°. The uncertainties in these values are a result of uncertainties in time and distance measurements. The neutron flight time versus distance is extrapolated to zero distance to determine the emission time for the most energetic neutrons.

The emission time and deuteron energy are compared with the time dependent accelerating voltage in Fig. 1. The ion energy trace in this figure corresponds to the measured diode voltage corrected for the drift tube inductance and reduced by the energy loss of the deuterons in traversing a thin foil used for current neutralization.[3] The maximum deuteron energy for this trace is 0.46 MeV in good agreement with the energy determination by TOF. The neutron emission time is determined relative to this ion energy trace through a fiducial timing pulse. This corresponds to a time of 87 ns on the ion energy trace in Fig. 1. This time must be reduced by the flight time of deuterons from the diode to the target (20 ns) to give the emission time of deuterons from the diode of 67 ± 7 ns as shown in Fig. 1. The uncertainty in this value results from propagating uncertainties in time and distance measurements. The deuteron emission time corresponds to the maximum deuteron energy within experimental error. Also there is no evidence

in the ion energy trace of more energetic deuterons emitted late in time which is consistent with the previous assumption that the most energetic neutrons are not emitted late in the pulse.

III. DEUTERON CURRENT

The time spread of the neutron response in a TOF detector is composed of three contributions: 1) the detector response, 2) the energy spread of the neutrons, and, 3) the duration of emission of the neutrons. The time spread of the responses in Fig. 1 is about 50 ns which is much larger than the detector response time. Since the width of the neutron response does not increase much with flight path, the time spread is determined in large part by the duration of neutron emission and not by the energy spread of the neutrons. The duration of neutron emission then provides a direct measure of the duration of the deuteron current.

1. Relation of Deuteron Current and TOF Yield

The time variation of the neutron yield $Y_n(t_n)$ is related to the time variation of the deuteron current $N_d(t)$ in the following way:

$$Y_n(t_n) = N_d(t) \int_o^{E_d} \sigma/\varepsilon dE \qquad (1)$$

where

$t_n = t + \ell_n/v_n + \ell_d/v_d$

ℓ_n = neutron flight path

v_n = neutron velocity

ℓ_d = deuteron flight path

$E_d = 1/2 m_d v_d^2$ = incident deuteron energy

σ = cross section for the $d(d,n)^3He$ reaction

ε = stopping cross section for deuterons in polyethylene

The neutron yield is related to the deuteron current through the reaction cross section integrated over the target thickness. It is assumed that the target thickness is larger than the range of the deuterons. The time of arrival of a neutron at the TOF detector (t_n) is different from the time that the deuteron was emitted from the diode by the flight time of the deuteron to the target (ℓ_d/v_d) and by the neutron flight time (ℓ_n/v_n). The slowing-down time of the deuterons in the target is negligible compared to the neutron flight time. It would appear that a measurement of the time variation of the neutron yield can be used to determine the deuteron current in time as long as the overtaking of slower neutrons by faster neutrons, i.e. orbit crossing, is not too severe.

In practice, the problem is complicated by two effects. First, the deuterons lose energy in the target so the outgoing neutrons have a velocity spread and hence a time spread. Since the cross section changes with deuteron energy, the neutron yield will change with the neutron energy or flight time. Second, for a configuration in which the ion beam is focused, there is a spread in angle for the deuterons incident on the target which produces a spread in angle for the outgoing neutrons. In our experiments, the half-angle for the focusing cone of deuterons on the target is about 35°. Since the cross section and neutron energy depend on the neutron emission angle, both a time spread of the outgoing neutrons and a variation in neutron yield arise from this angular spread.

The dependence of neutron energy on deuteron energy for different neutron emission angles is shown in Fig. 2. At small angles the neutron energy changes rapidly with deuteron energy,

but near 90° the neutron energy is less sensitive to the deuteron energy. If the deuteron beam is unidirectional on the target, as in an unfocused diode geometry, then the neutron time spread can be minimized by locating the detector near 90°.

The dependence of the cross section on deuteron energy and neutron emission angle is shown in Fig. 3. At all angles the cross section increases with deuteron energy. Consequently, the neutron response is largest for the most energetic neutrons and decreases in intensity toward longer time due to the deuteron energy loss in the target. Near 90°, the cross section is relatively insensitive to neutron angle so that in a focused geometry with angular spread, all angles will contribute nearly equally to the neutron response.

In our experiment, not only do we have the energy and angle variations discussed previously, but also the deuteron energy is time dependent due to the time variation of the diode voltage. For a neutron detector located at an angle θ_n relative to the deuteron beam direction, Eq. 1 can be rewritten to include these effects.

$$Y_n(t_n, \theta_n) = N_d(t) \int_o^{E_d(t)} \sigma(E, \theta_n)/\varepsilon(E)\, dE \qquad (2)$$

where $$t_n = t + \frac{\ell_n}{v_n} + \frac{\ell_d}{v_d}.$$

The neutron velocity is determined by the kinematics of the $d(d,n)^3He$ reaction for given values of E_d and θ_n. A straightforward inversion of Eq. 2 for deuteron current is not possible. Instead, the right side of Eq. 2 is calculated and compared with the measured neutron response. For this purpose, the corrected diode voltage trace is used for $E_d(t)$ and the deuteron current predicted by a simple analytic model[1] is used for $N_d(t)$.

Values of the reaction cross section (σ) and the stopping cross section (ϵ) are extracted from the literature. Center of mass differential cross sections for the $d(d,n)^3He$ reaction from 97 keV to 350 keV (Ref. 5) and from 300 keV to 700 keV (Ref. 6) were transformed to the laboratory system and fitted with smooth curves such as given in Fig. 3. These cross sections are based on measuring the outgoing ^3He particles. At higher energies, cross sections given by Brolley and Fowler[7] are used. These cross sections, which are based on neutron measurements, are consistent with values deduced from Ref. 6 below 700 keV except at the smallest angles (0° and 10°). For these angles the values of Brolley and Fowler are about 13% higher than values deduced from Ref. 6 and were normalized to the values from Ref. 6. Stopping cross sections for deuterons in polyethylene were calculated from stopping cross sections for protons in hydrogen and carbon taken from the recent compilation of Anderson and Ziegler.[8] Values of σ and ϵ which were used in evaluating neutron yields with Eq. 2 are listed in Table 1.

2. Measurements and Results

Neutron TOF measurements have been made with detectors located at 15° and 85° to the incident deuteron beam direction for flight paths of 1.91 m and 2.36 m respectively. Short flight paths are used to minimize the neutron time spread from energy variations. However, these flight paths are sufficiently long for the detectors to recover from the x-ray flash before recording neutrons. Results for a planar diode geometry without focusing are shown in Fig. 4. Here measured TOF responses are compared with yields calculated according to Eq. 2. The deuteron energy $E_d(t)$ and the deuteron current $N_d(t)$ for these calculations are given in Fig. 4. Neutron yields are calculated in 2 nsec time increments of $E_d(t)$ and $N_d(t)$ and then summed to give the curves which are plotted

as open points. The calculations have been normalized to the peaks of the measured responses.

To assess the importance of the duration of the current and energy pulses on the neutron response, a calculation was carried out using a monoenergetic deuteron pulse of constant current with a duration of only 2 nsec. Neutron responses calculated in this case are shown at the bottom of the figure. Here the temporal spread is larger at 15° than at 85° as expected from the cross section and kinematic variations discussed previously. However, at both angles these contributions are much less than the contribution from the duration of ion emission as given by the ion current and energy traces.

Results for the focused diode geometry are given in Fig. 5. In this geometry, the neutron angles range from 0° to 50° for the 15° detector and from 50° to 120° for the 85° detector. Neutron yields are calculated in 10° increments over these ranges according to Eq. 2 and summed to give the curves which are plotted as open points in Fig. 5. The deuteron energy $E_d(t)$ and deuteron current $N_d(t)$ used for these calculations are given in Fig. 5. Again the calculations have been normalized to the measured responses. Responses calculated for a monoenergetic deuteron pulse of 2 nsec duration are shown at the bottom of the figure. The larger temporal spreads of these responses than those in Fig. 4 indicate that the angular spread is limiting the temporal resolution significantly. Now the temporal spread is larger at 85° than at 15° as expected from the angular variations of the cross sections and kinematics discussed previously. Even with these temporal resolutions, the duration of the neutron TOF traces results primarily from the duration of ion emission as given by the ion-current and energy traces.

In making the comparison between calculated yields and measured TOF responses, it is assumed that the neutron

response is directly proportional to the neutron yield given by Eq. 2. The neutron response R_n is related to the neutron yield Y_n by the following expression.

$$R_n(t) = \Omega \varepsilon P Y_n(t)$$

where

Ω = solid angle of the neutron detector

ε = efficiency of the neutron detector

P = pulse-height response of the detector to neutrons.

The quantities ε and P are complicated energy-dependent properties of the neutron detector. The primary interaction process in the scintillator is n-p elastic scattering. In this case, the efficiency is proportional to the total n-p cross section and the pulse-height response depends on the proton-recoil energy, which is in fact a pulse-height distribution due to the variation in scattering angle of the recoil protons. An average over this distribution is made in the experiment because $\sim 10^6$ neutrons interact in each detector in a single shot. Then the quantity P corresponds to a pulse-height response averaged over the recoil-proton pulse-height distribution. Since this pulse-height response increases with neutron energy and the n-p cross section decreases with neutron energy in the energy range of interest, these variations tend to cancel each other. In the flat diode geometry, it is estimated that the net variation in the product of ε and P is $\leq 7\%$ for E_d ranging from 500 to 700 keV. In the focused diode geometry with a larger angular spread of the neutrons, the net variation in the product of ε and P is 15% for the 15° detector and 30% for the 85° detector for the same range of deuteron energies. Neutron interactions with carbon

in the scintillator have been ignored in making these estimates.

IV. CONCLUSIONS

Within experimental uncertainty, the time of emission of the most energetic neutrons corresponds to the production of the most energetic deuterons in the diode. In both the focused and unfocused geometries, the duration of the neutron response measured at either 15° or 85° to the anode to cathode direction results primarily from the duration of deuteron emission in the diode. In the focused geometry, the optimum time resolution is achieved at a small angle, but in the unfocused geometry, the time resolution is optimum at an angle near 90°. Finally, the shapes of the neutron yields calculated from an experimentally determined ion energy trace and a model dependent ion current trace are in reasonable agreement with the measured responses for both focused and unfocused geometries at both angles. This last result is especially important because time dependent ion currents are difficult to measure directly for the intense beams of interest. The agreement between the measured and calculated neutron yields supports the validity of the ion-production model used to unfold the ion current from measured electrical characteristics of the diode.

REFERENCES

1. S.J. Stephanakis, D. Mosher, G. Cooperstein, J.R. Boller, J. Golden and S.A. Goldstein, Phys. Rev. Lett. 37, 1543 (1976).

2. F.C. Young, J. Golden and C.A. Kapetanakos, Rev. Sci. Instrum. 48, 432 (1977).

3. D. Mosher, G. Cooperstein, S.J. Stephanakis, S.A. Goldstein, D.G. Colombant and R. Lee, 2nd. Int. Conf. on High Power Electron and Ion Beam Res. and Tech., Cornell University, Ithaca, New York, 1977, p. 257; Also NRL Memorandum Report 3658 (Washington, D.C., November 1977); and S.A. Goldstein, G. Cooperstein, R. Lee, D. Mosher and S.J. Stephanakis, Phys. Rev. Lett. 40, 1504 (1978).

4. F.C. Young and S.J. Stephanakis, NRL Memorandum Report 3104 (Washington, D.C., August 1975).

5. R.B. Theus, W.I. McGarry and L.A. Beach, Nucl. Phys. 80, 273 (1966).

6. N. Ying, B.B. Cox, B.K. Barnes and A.W. Barrows, Jr., Nucl. Phys. A206, 481 (1973).

7. J.E. Brolley, Jr. and J.L. Fowler in Fast Neutron Physics, Eds. J.B. Marion and J.L. Fowler, Part 1 (Wiley-Interscience, New York, 1960), p. 73.

8. H.H. Andersen and J.F. Ziegler, The Stopping and Ranges of Ions in Matter, Vol. 3 (Pergamon Press, New York, 1977).

Table 1

Values of $\epsilon(10^{-15}$ eV-cm$^2)$ for deuterons on polyethylene

and σ(mb) for the $d(d,n)^3He$ reaction

E_d (keV)	ϵ	$\sigma(0°)$	$\sigma(10°)$	$\sigma(20°)$	$\sigma(30°)$	$\sigma(40°)$	$\sigma(50°)$	$\sigma(60°)$	$\sigma(70°)$	$\sigma(80°)$	$\sigma(90°)$	$\sigma(100°)$	$\sigma(110°)$	$\sigma(120°)$
50		1.3	1.2	1.1	1.0	0.95	0.85	0.75	0.65	0.60	0.60	0.60	0.65	0.70
100	27.4	2.7	2.6	2.4	2.2	2.0	1.7	1.45	1.3	1.2	1.15	1.2	1.25	1.35
150	27.5	4.6	4.4	4.0	3.6	3.1	2.6	2.15	1.85	1.65	1.65	1.7	1.8	2.0
200	26.1	6.4	6.2	5.6	4.95	4.1	3.35	2.75	2.4	2.15	2.1	2.15	2.35	2.6
250	24.2	8.15	7.85	7.15	6.15	5.0	4.05	3.3	2.75	2.5	2.4	2.5	2.8	3.15
300	22.3	9.9	9.5	8.55	7.15	5.8	4.6	3.7	3.1	2.75	2.7	2.8	3.1	3.55
350	20.7	11.35	10.9	9.7	8.05	6.5	5.1	4.05	3.35	3.0	2.95	3.1	3.4	3.9
400	19.4	12.7	12.1	10.75	8.9	7.05	5.5	4.35	3.55	3.2	3.15	3.3	3.65	4.2
450	18.1	13.9	13.3	11.7	9.7	7.6	5.9	4.6	3.8	3.4	3.35	3.5	3.9	4.5
500	17.0	15.1	14.5	12.7	10.4	8.1	6.25	4.8	4.0	3.6	3.55	3.7	4.15	4.8
550	16.1	16.3	15.6	13.7	11.1	8.6	6.6	5.05	4.2	3.8	3.75	3.9	4.35	5.05
600	15.2	17.5	16.7	14.6	11.8	9.0	6.8	5.25	4.4	4.0	3.9	4.1	4.55	5.25
650	14.5	18.6	17.8	15.5	12.4	9.4	7.1	5.4	4.55	4.15	4.05	4.25	4.7	5.45
700	13.8	19.8	18.8	16.3	13.0	9.8	7.3	5.6	4.75	4.3	4.2	4.4	4.85	5.6
750	13.2	20.9	19.8	17.2	13.4	10.1	7.5	5.75	4.85	4.4	4.25	4.55	5.0	5.7
800	12.7	21.9	20.9	18.0	13.8	10.4	7.7	5.9	4.9	4.45	4.35	4.6	5.15	5.85
850	12.2	22.9	21.9	18.7	14.2	10.6	7.9	6.0	4.9	4.5	4.35	4.7	5.25	5.95
900	11.7	23.8	22.8	19.3	14.6	10.8	8.0	6.1	4.95	4.5	4.4	4.75	5.35	6.05

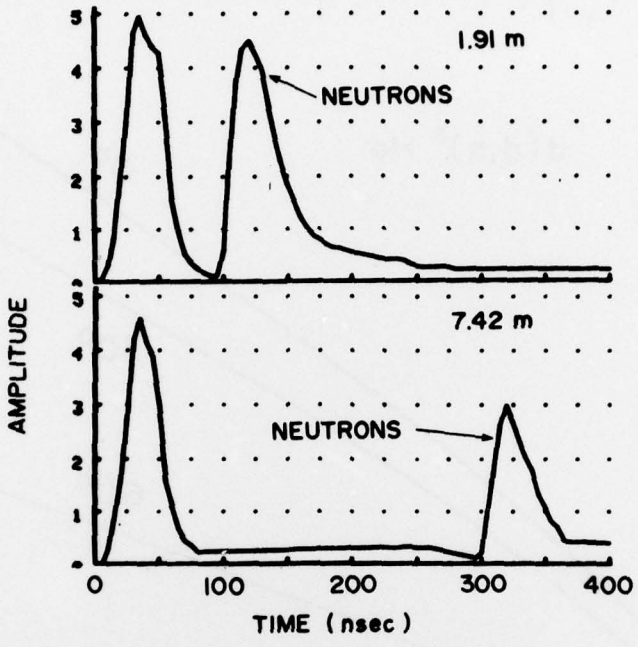

MAXIMUM DEUTERON ENERGY = (0.45 ±0.1) MeV

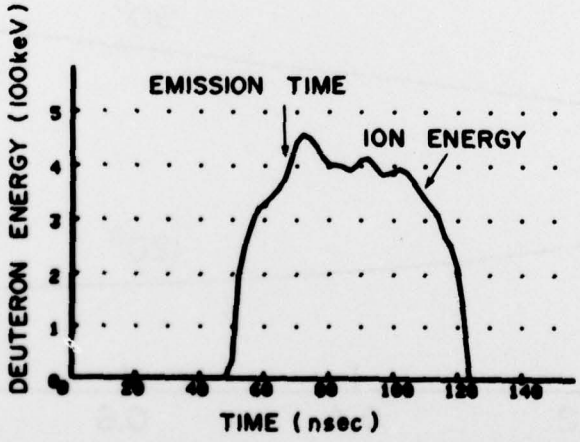

TIME OF EMISSION OF MAXIMUM ENERGY DEUTERONS = (67 ±7) nsec

Fig. 1 — Neutron TOF measurements for two detectors at 15° to the diode axis and at flight paths at 1.91 m and 7.42 m respectively. The maximum deuteron energy corresponds to the most energetic neutrons which are detected at the leading edge of the TOF traces. On the bottom of this figure, the emission time of these deuterons from the diode is compared with the ion-energy trace.

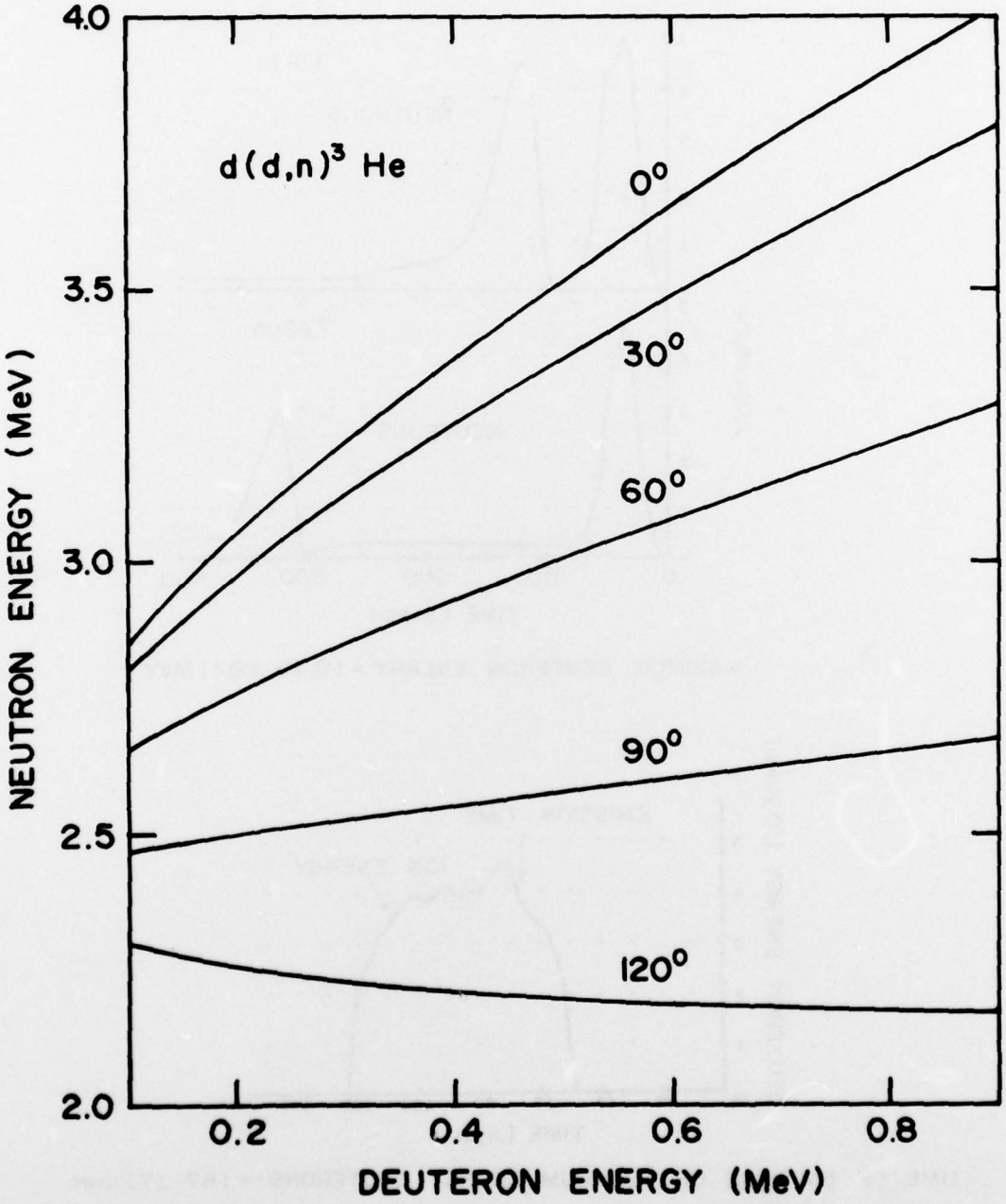

Fig. 2 — Dependence of outgoing neutron energy on incident deuteron energy for the $d(d,n)^3He$ reaction for neutron emission angles ranging from 0° to 120°.

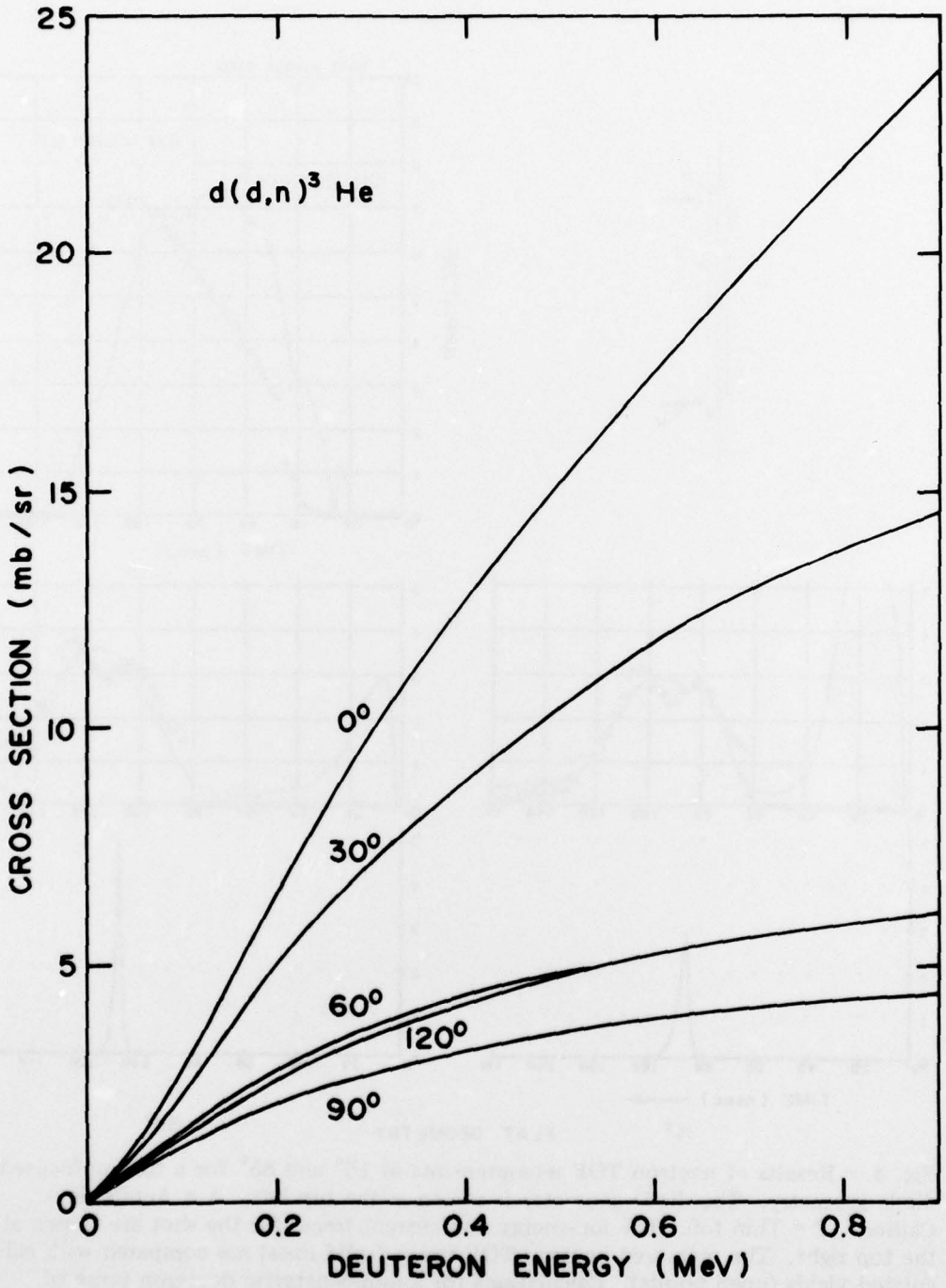

Fig. 3 — Dependence of the $d(d,n)^3He$ reaction cross section on incident deuteron energy for neutron-emission angles ranging from 0° to 120°.

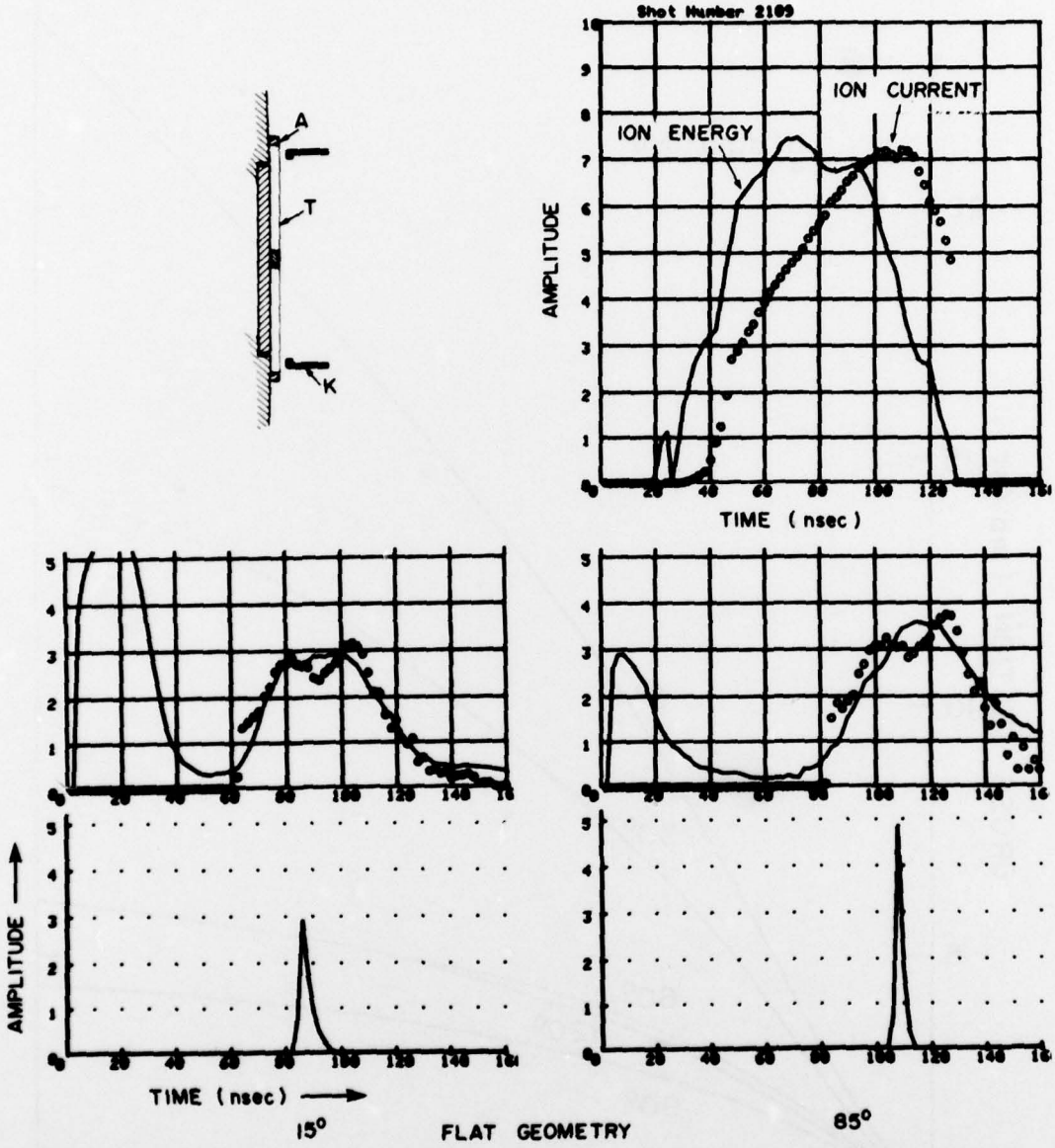

Fig. 4 — Results of neutron TOF measurements at 15° and 85° for a flat (unfocused) diode geometry. The diode geometry is shown at the top left: A = Anode, K = Cathode, T = Thin foil. The ion-energy and current traces for the shot are shown at the top right. The measured neutron TOF traces (solid lines) are compared with calculated yields (open points). Calculations for a monoenergetic deuteron pulse of 2 nsec duration are given at the bottom of the figure.

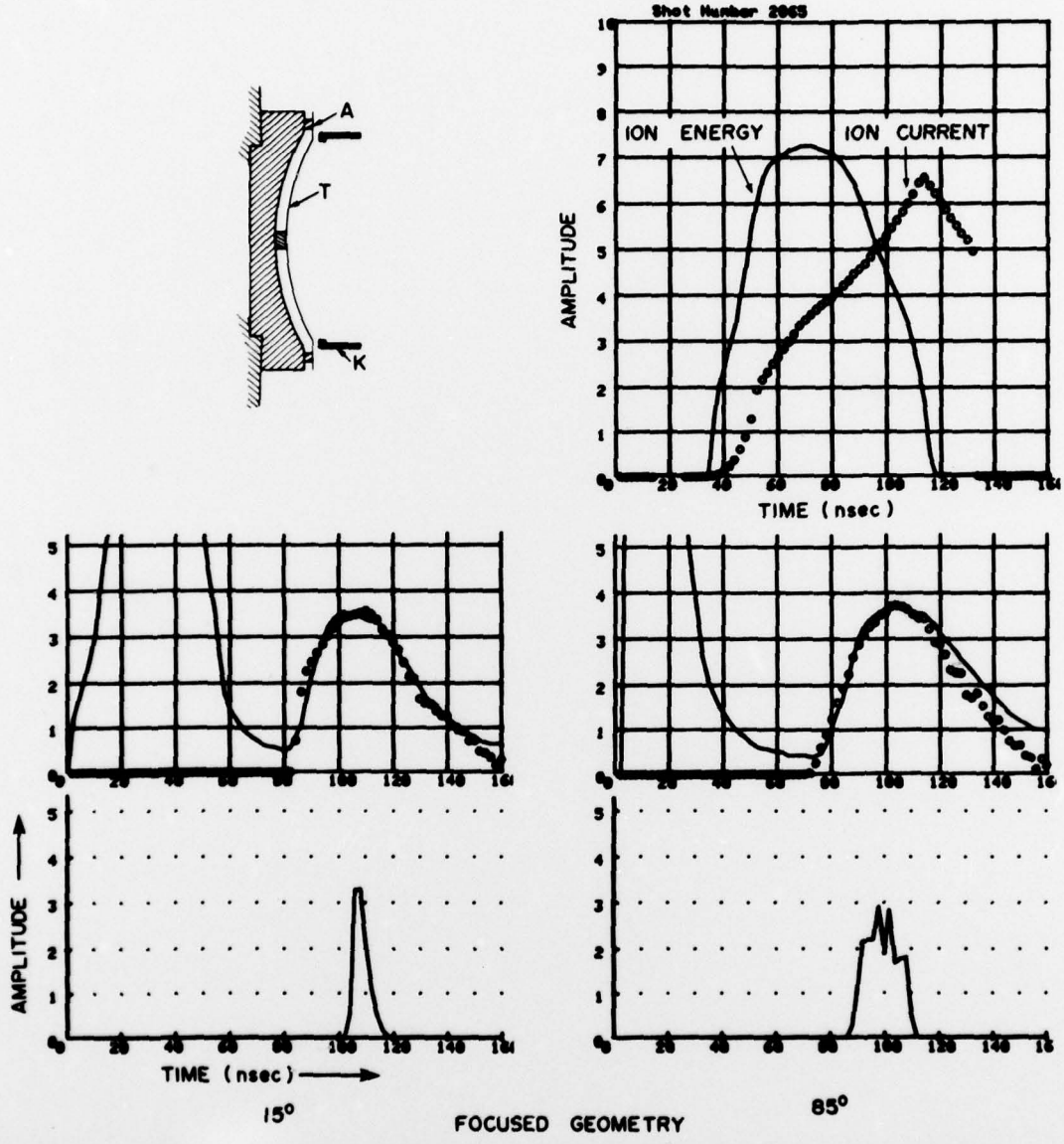

Fig. 5 — Results of neutron TOF measurements at 15° and 85° for a focused-diode geometry. The diode geometry is shown at the top left: A = Anode, K = Cathode, T = Thin foil. The ion-energy and current traces for this shot are shown at the top right. Measured neutron TOF traces (solid lines) are compared with calculated yields (open points). Calculations for a monoenergetic deuteron pulse of 2 nsec duration are given at the bottom of the figure.

TEMPORAL DEUTERON CURRENT DETERMINATIONS
USING NEUTRON TIME-OF-FLIGHT

Director
Defense Advanced Research Projects Agency
Architect Building
1400 Wilson Boulevard
Arlington, VA 22209
Attn: LTC R.P. Sullivan 1

Director
Defense Nuclear Agency
Washington, D.C. 20305
Attn: DDST, Mr. Peter Haas 1

Director
Defense Nuclear Agency
Washington, D.C. 20305
Attn: RATN 1

Director
Defense Nuclear Agency
Washington, D.C.
Attn: STTL, Technical Library 2

Director
Defense Nuclear Agency
Washington, D.C. 20305
Attn: RAEV 2

Director
Defense Nuclear Agency
Washington, D.C. 20305
Attn: STVL 1

Director
Defense Nuclear Agency
Washington, D.C. 20305
Attn: STSI 1

Commander
Field Command
Defense Nuclear Agency
Albuquerque
Kirtland AFB, New Mexico 87115
Attn: FCPR 1

Chief
Field Command
Defense Nuclear Agency
Livermore Division
Box 808
Livermore, California 94550
  Attn: FCPR-L 1

Director
Defense Research and Engineering
Washington, D.C. 20301
  Attn: DAD (SK)Mr. G.R. Barse 1

Commander
Harry Diamond Laboratories
2800 Powder Mill Road
Adelphi, MD 20783
  Attn: AMXDO-RBF, Mr. John Rosado 1

Commander
Harry Diamond Laboratories
2800 Powder Mill Road, Adelphi, MD 20783
  Attn: AMXDO-RBH, Mr. S. Graybill 1

Commander
Harry Diamond Laboratories
2800 Powder Mill Road
Adelphi, MD 20783
  Attn: AMXDO-RC, Dr. Robert Oswald, Chief, LAB 300 1

Air Force Weapons Laboratory, AFSC
Kirtland AFB, New Mexico 87117
  Attn: DY, Dr. Guenther 1

Air Force Weapons Laboratory, AFSC
Kirtland AFB, New Mexico 87117
  Attn: EL, Mr. John Darrah 1

Air Force Weapons Laboratory, AFSC
Kirtland AFB, New Mexico 87117
  Attn: DYS, Dr. Baker 1

Air Force Weapons Laboratory, AFSC
Kirtland AFB, New Mexico 87117
  Attn: SAA 1

Air Force Weapons Laboratory, AFSC
Kirtland AFB, New Mexico 87117
  Attn: SUL, Technical Library 1

Air Force Weapons Laboratory, AFSC
Kirtland AFB, New Mexico 87117
  Attn: ELP, TREE Section 1

Space and Missile Systems Organization
Post Office Box 92960
Worldway Postal Center
Los Angeles, CA 90009
Attn: SKT, Mr. Peter H. Stadler 1

Space and Missile Systems Organization
P.O. Box 92960
Worldway Postal Center
Los Angeles, CA 90009
Attn: RSP, System Defense and Assessment,
LTC Gilbert 1

Sandia Laboratories
P.O. Box 5800
Albuquerque, N.M. 87115
Attn: Document Control for 5220, Dr. J.V. Walker 1

Sandia Laboratories
P.O. Box 5800
Albuquerque, N.M. 87115
Attn: Document Control for 5242, Dr. G. Yonas 1

Sandia Laboratories
P.O. Box 5800
Albuquerque, N.M. 87115
Attn: Document Control for Technical Library 1

Aerospace Corporation
P.O. Box 92957
Los Angeles, CA 90009
Attn: Mr. J. Benveniste 1

Aerospace Corporation
P.O. Box 92957
Los Angeles, CA 90009
Attn: Dr. Gerald G. Comisar, Jr. 1

University of Texas
Fusion Research Center
Physics Building 330
Austin, TX 78712
Attn: Dr. William E. Drummond 1

Battelle Memorial Institute
Columbus Laboratories
505 King Avenue
Columbus, Ohio 43201
Attn: Mr. P. Malozzi 1

Maxwell Laboratories, Inc.
9244 Balboa Avenue
San Diego, CA 92123
Attn: Dr. P. Korn 1

Mission Research Corporation
735 State Street
Santa Barbara, CA 93101
Attn: Dr. Conrad L. Longmire 1

Physics International Corporation
2700 Merced Street
San Leandro, CA 94577
Attn: Document Control for Dr. Sidney Putnam 1

Physics International Corp.
2700 Merced Street
San Leandro, CA 94577
Attn: Document Control for Mr. Ian Smith 1

R & D Associates
P.O. Box 9695
Marina del Rey, CA 90291
Attn: Dr. Bruce Hartenbaum 1

Science Applications, Inc.
P.O. Box 2351
La Jolla, CA 92037
Attn: Dr. J. Robert Beyster 1

Stanford Research Institute
333 Ravenswood Avenue
Menlo Park, CA 94025
Attn: Dr. Robert A. Armistead, Jr. 1

Dr. Victor A.J. Van Lint
Mission Research Corporation
7650 Convoy Court
San Diego, CA 92111 1

Commander
Naval Surface Weapons Center
White Oak Laboratory
Silver Spring, MD 20910 1

DASIAC, GE Tempo
El Paseo Building
816 State Street
Santa Barbara, CA 93102 1

Jaycor
205 South Whiting
Suite 500
Alexandria, VA 22304 1

AFOSR/NP
Capt. R.L. Gullickson
Bolling AFB, Washington, DC 20332 1

Dr. Alan Bomborsky Harry Diamond Laboratories 2800 Powder Mill Road Adelphi, MD 20783	1
Dr. A.E. Blaugrund Weizmann Institute of Science Rehovot, Israel	1
Dr. J.E. Maenchen Division 8220 Physics International Corp. 2700 Merced Street San Leandro, CA 94577	1
CEA, Centre de Etudes de Limeil Dr. Alain Jolas B.P. 27 94190 - Villeneuve - Saint George, France	1
DDC	12
Code 2628	20
Code 6770	20
Code 6700	1
Code 6600	1
Code 6770-Dr. D. Mosher	10
Code 6770-S.J. Stephanakis	10
Code 6770-S. Goldstein	10
Code 6770-D. Hinshelwood	10
Code 6603M Dr. K.W. Marlow	1
Code 6603M Dr. F.C. Young Balance of Run	59
	200